

1       **Genome compartmentalization predates species divergence in the plant pathogen**

2       **genus *Zymoseptoria***

3

4       Alice Feurtey<sup>1,2\*</sup>, Cécile Lorrain<sup>1,2,3\*</sup>, Daniel Croll<sup>4</sup>, Christoph Eschenbrenner<sup>1,2</sup>, Michael Freitag<sup>5</sup>,

5       Michael Habig<sup>1,2</sup>, Janine Haueisen<sup>1,2</sup>, Mareike Möller<sup>1,2,5</sup>, Klaas Schotanus<sup>1,2,6</sup>, and Eva H.

6       Stukenbrock<sup>1,2</sup>

7

8

9       Affiliations:

10      <sup>1</sup> Environmental Genomics, Max Planck Institute for Evolutionary Biology, 24306 Plön, Germany

11      <sup>2</sup> Environmental Genomics, Christian-Albrechts University of Kiel, 24118 Kiel, Germany

12      <sup>3</sup> INRA Centre Grand Est - Nancy, UMR 1136 INRA/Université de Lorraine Interactions

13      Arbres/Microorganismes, Champenoux 54280, France

14      <sup>4</sup> Laboratory of Evolutionary Genetics, Institute of Biology, University of Neuchâtel, 2000  
15      Neuchâtel, Switzerland.

16      <sup>5</sup> Department of Biochemistry and Biophysics, Oregon State University, Corvallis, OR, USA

17      <sup>6</sup> Department of Molecular Genetics and Microbiology, Duke University, Duke University Medical  
18      Center, Durham, NC 27710, USA

19

20      \*Authors contributed equally to the work. Correspondence: Alice Feurtey

21      ([feurtey@evolbio.mpg.de](mailto:feurtey@evolbio.mpg.de)), Cécile Lorrain ([lorrain@evolbio.mpg.de](mailto:lorrain@evolbio.mpg.de))

22

23      **Abstract**

24      **Background:** Antagonistic co-evolution can drive rapid adaptation in pathogens and shape  
25      genome architecture. Comparative genome analyses of several fungal pathogens revealed  
26      highly variable genomes, for many species characterized by specific repeat-rich genome  
27      compartments with exceptionally high sequence variability. Dynamic genome architecture may

28 enable fast adaptation to host genetics. The wheat pathogen *Zymoseptoria tritici* with its highly  
29 variable genome and has emerged as a model organism to study the genomic evolution of plant  
30 pathogens. Here, we compared genomes of *Z. tritici* isolates and genomes of sister species  
31 infecting wild grasses to address the evolution of genome composition and structure.

32 **Results:** Using long-read technology, we sequenced and assembled genomes of *Z. ardabilliae*,  
33 *Z. brevis*, *Z. pseudotritici* and *Z. passerinii*, together with two isolates of *Z. tritici*. We report a  
34 high extent of genome collinearity among *Zymoseptoria* species and high conservation of  
35 genomic, transcriptomic and epigenomic signatures of compartmentalization. We identify high  
36 gene content variability both within and between species. In addition, such variability is mainly  
37 limited to the accessory chromosomes and accessory compartments. Despite strong host  
38 specificity and non-overlapping host-range between species, effectors are mainly shared among  
39 *Zymoseptoria* species, yet exhibiting a high level of presence-absence polymorphism within *Z.*  
40 *tritici*. Using *in planta* transcriptomic data from *Z. tritici*, we suggest different roles for the shared  
41 orthologs and for the accessory genes during infection of their hosts.

42 **Conclusion:** Despite previous reports of high genomic plasticity in *Z. tritici*, we describe here a  
43 high level of conservation in genomic, epigenomic and transcriptomic signatures of genome  
44 architecture and compartmentalization across the genus *Zymoseptoria*. The compartmentalized  
45 genome may reflect purifying selection to retain a functional core genome and relaxed selection  
46 on the accessory genome allowing a higher extent of polymorphism.

47

48 **Keywords:** *genome evolution, orphan genes, effectors, genome architecture, accessory genes*

49 **Introduction**

50 Co-evolution between plants and pathogens can drive rapid evolution of genes involved in  
51 antagonistic interaction [1]. In filamentous plant pathogens, rapid evolution may be fueled by  
52 highly dynamic genome architecture involving repeat-rich compartments such as gene-sparse  
53 islands of repetitive DNA and accessory chromosomes [2, 3]. These compartments can show a  
54 high plasticity revealed by a high extent of gene and/or chromosome presence-absence

55 variation and structural variants, such as inversions, insertions and deletions [4, 5]. Several plant  
56 pathogenic fungi have isolate specific chromosomes, so-called accessory chromosomes.

57

58 Accessory chromosomes are characterized by intra-species presence-absence polymorphism,  
59 low gene density, an enrichment of repetitive sequences and, in some species, a different  
60 histone methylation pattern [6, 7]. It has been shown that accessory chromosomes encode  
61 genes involved in virulence such as in the species *Fusarium solani*, *Fusarium oxysporum* and  
62 *Leptosphaeria maculans* [8–11]. Little is known about the evolutionary origin of accessory  
63 chromosomes although experimental evidence from the asexual species *F. oxysporum* shows  
64 that accessory chromosomes may be acquired horizontally as chromosomes can be transferred  
65 between distinct isolates by hyphal fusion [10]. Through such transfers, virulence determinants  
66 may be exchanged between clonal lineages as accessory chromosomes in this species were  
67 shown to encode host specific virulence determinants and transcription factors regulating their  
68 expression [12].

69

70 Genes involved in plant-pathogen interactions may diversify at a higher rate in repeat-rich  
71 genome compartments and thereby evolve new virulence specificity faster [3]. These genes  
72 encode secreted proteins, so-called effectors [1]. Most known effectors target diverse cellular  
73 compartments and molecular pathways, including immune response-related pathways [13, 14].  
74 Genes encoding Carbohydrate-active enzymes (CAZymes) have also been associated to the  
75 pathogenic lifestyle of fungal plant pathogens, particularly through their role in plant-cell wall  
76 degradation [15]. Thus, some secreted CAZymes may be essential from the early infection  
77 stage, like penetration of plant tissue, to later stages such as the necrotrophic phase where the  
78 pathogen feed from dead plant tissue [16]. Likewise, secondary metabolites are known to be  
79 involved in plant infection and contribute to virulence and the interaction with other plant-  
80 associated microorganisms [17, 18]. Many of these genes can be predicted either according to  
81 their composition and known protein domains or through machine learning methods [19].  
82 Thereby, in-depth genome annotations have proven important to predict and compare the

83 content of pathogenicity-related genes in plant pathogens, as well as their genomic localization  
84 for example in rapidly evolving genome compartments.

85

86 The ascomycete pathogen *Zymoseptoria tritici* has emerged as a model organism in  
87 evolutionary genomics of pathogens. This species originated in the Fertile Crescent during the  
88 domestication of its host, wheat [20]. Closely related species of *Z. tritici* have been collected  
89 from wild grasses in the Middle East providing an excellent resource for comparative genome  
90 analyses of closely related and recently diverged pathogen species. Comparative analyses of  
91 genome organization and gene content within and among *Zymoseptoria* species have previously  
92 revealed a wide distribution of accessory chromosomes and dynamic gene content [21, 22]. The  
93 haploid genome of the reference isolate IPO323 comprises thirteen core and eight accessory  
94 chromosomes [23]. Some of these accessory chromosomes encode traits that impact virulence  
95 of the fungus, however no gene encoded on an accessory chromosome has so far been  
96 described as a virulence or avirulence determinant [24–29]. Interestingly, the accessory  
97 chromosomes in *Z. tritici* show a low transcriptional activity *in vitro* as well as *in planta* [30, 31].  
98 This suppression of gene expression correlates with an enrichment of heterochromatin  
99 associated with the histone modification H3K27me3 on the accessory chromosomes [6, 32].

100

101 In the reference isolate IPO323, the accessory chromosomes comprise more than 12% of the  
102 entire genome assembly. To which extent such a high amount of accessory DNA is also found in  
103 genomes of other members of the *Zymoseptoria* genus has so far been unknown due to the lack  
104 of high-quality genome assemblies and large scale population sequencing. Assemblies based  
105 on short-read data failed to recover complete sequence of accessory chromosomes and “orphan  
106 regions” due to their high repeat content [22]. The asset of genome assemblies based on long-  
107 read sequencing was demonstrated in a detailed genome comparison of four *Z. tritici* isolates  
108 sequenced with PacBio long-read sequencing [28]. Comparison of the high-quality chromosome  
109 assemblies revealed the occurrence of “orphan regions” enriched with transposable elements  
110 and encoding putative virulence-related genes [33].

111

112 In this study, we investigate the genomic architecture and variability among five *Zymoseptoria*  
113 genomes. Beside presenting a new and significantly improved resource for future genomic  
114 studies of these fungal pathogens, we specifically ask: 1) how conserved is the genome  
115 architecture among *Zymoseptoria* species, 2) can we identify accessory compartments in other  
116 *Zymoseptoria* isolates and 3) to which extent does variation in genome architecture reflect  
117 variation in gene content.

118 To answer these questions, we used high-quality assemblies based on long-read sequence data  
119 and new gene predictions in two isolates of *Z. tritici* (Zt05 and Zt10) and one isolate of each of  
120 the sister species, *Z. ardabilliae*, *Z. brevis*, *Z. passerinii*, and *Z. pseudotritici*. We explore the core  
121 and non-core genome architecture of *Zymoseptoria* spp. combining genomic data with  
122 transcriptome and histone methylation data and relate this to core and accessory genome  
123 compartments. Furthermore, we compare the distribution of orthologous and non-orthologous  
124 genes in the *Zymoseptoria* genomes and one additional Dothideomycete species. Our analyses  
125 reveal an overall conserved genome architecture characterized by gene-rich core compartments  
126 and accessory compartments enriched in species-specific genes. Finally, we report an  
127 exceptionally high extent of variation in presence-absence of protein coding genes in a  
128 eukaryote genome.

129 **Results**

130 **New de novo assemblies using long-read sequencing for six *Zymoseptoria* spp.**

131 We sequenced and assembled the genome of the reference isolates of *Z. ardabilliae*, *Z. brevis*,  
132 *Z. pseudotritici* and *Z. passerinii* and the genomes of two *Z. tritici* isolates sampled in Denmark  
133 and Iran. The obtained contigs were filtered based on base-quality confidence and read depth to  
134 ensure high quality of the final assemblies (see Methods). This filter removed a high number of  
135 contigs (between 17% and 58% of the total), but little overall length (between 0.4 and 2.6% of  
136 the total assemblies), indicating that most of the excluded contigs were of small size. The best

137 assemblies were of the two *Z. tritici* isolates comprising 19 and 30 contigs and the most  
138 fragmented was of *Z. passerinii* comprising 103 contigs (Figure 1). The resulting assembly  
139 lengths ranged from 38.1 Mb for *Z. ardabiliiae* to 41.6 Mb for *Z. brevis*, which is comparable to  
140 the reference assembly length of *Z. tritici* (39.7 Mb) but slightly larger than previous short-read  
141 based assemblies (Table 1; previous assemblies ranged from 31.5 *Z. ardabiliiae* to 32.7 for *Z.*  
142 *pseudotritici* [22, 23]. The assembly of the Iranian *Z. tritici* isolate Zt10 has telomeric repeats at  
143 the end of all contigs, indicating that each chromosome is completely assembled, comprising six  
144 accessory and thirteen core chromosomes. The assemblies for the Danish *Z. tritici* isolate  
145 (Zt05), *Z. brevis* (Zb87) and *Z. pseudotritici* (Zp13) contained, respectively, twelve, nine and five  
146 fully assembled chromosomes including both core and accessory chromosomes (Figure S1).  
147 The assemblies of the *Z. ardabiliiae* (Za17) and *Z. passerinii* (Zpa63) genomes included no fully  
148 assembled chromosomes, but twelve and ten contigs respectively with telomeres at one of the  
149 ends (Table 1; Figure S1).

150 The transcriptome-based gene predictions for these new assemblies include between 10,528  
151 and 12,386 protein-coding genes (Table S1). This range is consistent with the annotation of the  
152 reference genome IPO323 reporting 11,839 protein-coding genes [22]. We used Benchmarking  
153 Universal Single-Copy Orthologs (BUSCO) from the lineage dataset *Pezizomycotina* to evaluate  
154 the completeness of the assemblies and gene predictions (Waterhouse et al. 2018). The  
155 proportion of complete BUSCOs were as follow Zt10: 98.7%, Zt05: 98.4%, Zp13: 98.5%, Zb87:  
156 97.0%, Za17: 98.2% and Zpa63: 97.5%. These values are comparable to the one obtained for  
157 the reference genome of *Z. tritici* (97.8%). The assessment of gene content completeness (see  
158 Methods) indicates that, despite more fragmented assemblies of *Z. ardabiliiae* and *Z. passerinii*,  
159 the genomes are complete in terms of gene content and that the unassembled fragments are  
160 more likely to comprise repeats and not protein coding genes.

161 Based on the whole-genome sequences and the predicted genes we reconstructed the  
162 phylogeny of the *Zymoseptoria* genus using the publicly available genome of *Cercospora*  
163 *beticola* as an outgroup [34, 35]. For both trees, the phylogenetic relationship of the

164 *Zymoseptoria* species is in accordance with previously published phylogeny based on seven loci  
165 sequenced in multiples isolates (Figure 1) [21].

166 **Genomes of *Zymoseptoria* spp. comprise accessory chromosomes and compartments**  
167 **but show overall high synteny**

168 Next we addressed the extent of co-linearity of the *Zymoseptoria* genomes. Using coordinates of  
169 orthologous genes, we were able to reveal a high extent of synteny conservation among the five  
170 *Zymoseptoria* species and between the three isolates of *Z. tritici*, as depicted in Figures 2 and  
171 S2. Based on this high extent of synteny and the prediction of telomeric repeats, we identified  
172 the correspondence of chromosomes between the reference genome of *Z. tritici* IPO323 and the  
173 other *Zymoseptoria* genomes (Figure 2 and S2). *Z. brevis* and *Z. pseudotritici* share a near  
174 perfect synteny in their core chromosomes, however, when compared to *Z. tritici*, *Z. brevis* and  
175 *Z. pseudotritici* have two large-scale inversions comprising roughly ~900 kb and ~1.2 Mb of  
176 chromosomes 2 and 6, respectively (Figure 2, S2 and S3). Based on the phylogeny in Figure 1,  
177 it is likely that these two events occurred after the divergence of *Z. tritici* from *Z. brevis* and *Z.*  
178 *pseudotritici*. Overall, we observe a higher extent of synteny conservation between *Z. brevis* and  
179 *Z. pseudotritici* compared to *Z. tritici* IPO323 (Figure 2; S2 and S3).

180 In *Z. tritici*, core and accessory compartments have very distinct genomic features. It was  
181 previously shown that hallmarks of accessory regions in the reference isolate IPO323 include  
182 lower gene density, lower levels of H3K4 methylation levels and lower gene expression [6, 31].  
183 In the reference genome of IPO323, compartments with these genomic and epigenomic  
184 hallmarks represent either accessory chromosomes or specific regions of the core  
185 chromosomes. Here we find that the specific accessory hallmarks including low gene density,  
186 low expression, low H3K4me2 methylation and significant enrichment of species-specific genes  
187 (see description below) on the non-core contigs are found in genomic compartments throughout  
188 the genus (Table S3, Figures 3 and S4).

189 In the reference *Z. tritici* strain, the specific “accessory-like” pattern includes a particular region  
190 of the core chromosome 7 of ~0.6 Mb (Figure 3A) [6]. This particularly large accessory marked

191 region is observed in several *Zymoseptoria* spp (Figure 3B; S4). We identify ~0.7 Mb of the  
192 contig 28 in *Z. pseudotritici* and ~0.6 Mb of the contig 17 for *Z. brevis*, both corresponding to  
193 chromosome 7 of *Z. tritici*, which share the same hallmarks of accessory chromosomes (Figures  
194 3 and S4, Table S3). For the two remaining sister species, the fragmentation of the assembly  
195 does not allow the identification of such pattern although there is an indication of a similar effect  
196 on gene expression and species-specific gene enrichment on contig 19 of *Z. ardabilliae* which  
197 corresponds to a fragment of chromosome 7 in IPO323 (Figure S5).

198 We also identified other regions enriched in isolate-specific genes, thus defining orphan loci in  
199 the core chromosomes of both Zt10 and Zt05 (Figures 3 and S4). We observe a region of ~0.2  
200 Mb of contig 1 in the Iranian isolate Zt10 corresponding to the core chromosome 3 in the IPO323  
201 genome with high content of isolate-specific genes (Figure S4; table S3). We furthermore  
202 identified small segments with species-specific genes on the core chromosomes of the wild-  
203 grass infecting sister species including a ~0.3 Mb region of the contig 26 in *Z. brevis* and ~0.1  
204 Mb of contig 30. Overall, we show that genome compartmentalization in core and accessory  
205 regions is an ancestral and shared trait among the *Zymoseptoria* species. This phenomenon  
206 generates highly variable compartments and defined loci that deviate from genome averages in  
207 terms of gene content, sequence composition and synteny conservation.

208 **Variable repertoires of effector candidate genes**

209 To obtain gene annotations for the *Zymoseptoria* genome assemblies, we established a custom  
210 pipeline adapted from Lorrain and co-workers (Figure S5) [36]. Briefly, we use the consensus of  
211 three methods to predict gene product localization, then extract secreted proteins to further  
212 identify predicted effectors. This detailed functional annotation provided a catalog of predicted  
213 gene functions and cellular localizations (Figure S6). For each genome, a large proportion of  
214 genes could not be assigned to a protein function and lacked protein domains. 49.6% of genes  
215 in *Z. tritici* (N = 5953) and up to 71.8% of genes in *Z. pseudotritici* (N = 8373) lack a predicated  
216 function (Figure S6A). A relatively consistent number of genes are predicted for each functional  
217 category among *Zymoseptoria* spp. (Figure S6A and B). Likewise, the numbers of gene products

218 predicted to belong to the different subcellular localizations are very similar (Figure S6C) across  
219 the whole genus, including secreted proteins. The difference between the minimal and maximal  
220 gene number fpr the different categories of subcellular localizations do not exceed 1.6X between  
221 species (Figure S6C). Overall, secretomes range from 7% of the genes predicted in *Z. passerinii*  
222 (N=828) to 11% of genes in *Z. ardabilliae* (N=1328 genes, Figure S6B).  
223 We further investigated the number and distribution of genes predicted to encode proteins with a  
224 pathogenicity-related function, such as secondary metabolites, CAZymes and effector  
225 candidates (Figures S1 and S6B). Genes involved in the synthesis of secondary metabolites are  
226 typically organized in clusters, with genes participating in the same biosynthetic pathway  
227 grouping together at a genomic locus (Shi-Kunne et al. 2019). The number of biosynthetic gene  
228 clusters (BGC) ranges from 25 in *Z. ardabilliae* and *Z. passerinii* to 33 in the IPO323 reference  
229 genome and includes from 305 to 471 predicted genes (Figure S1). The only BGC identified in a  
230 non-core contig is a non-ribosomal peptide synthetase BGC found on the contig 38 of *Z. brevis*  
231 which has no orthologous cluster detected in any of the other *Zymoseptoria* genomes (Figure  
232 S1). We identified between 454 and 515 CAZyme genes in the *Zymoseptoria* species. Both  
233 BGCs and CAZymes are almost exclusively found on the core chromosomes (Figure S1). The  
234 only exceptions are a CAZyme encoding gene found on chromosome 14 in *Z. tritici* IPO323 and  
235 Zt05, and a CAZyme encoding gene on the putative accessory contig 38 of *Z. brevis* (Figure  
236 S1). These two genes encode for a beta-glucosidase and a carboxylic-ester hydrolase,  
237 respectively.  
238 In contrast to the high conservation of CAZyme and BGC gene content among the *Zymoseptoria*  
239 genomes, we find that predicted effector genes exhibit a large variation in gene numbers  
240 between genomes (Figure S6B). In fact, the predicted effector gene repertoire of in *Z. ardabilliae*  
241 (N=637) is three times as high compared to *Z. brevis* (N=206). Interestingly, the three *Z. tritici*  
242 isolates also vary considerably in their predicted effector repertoires. The reference isolate  
243 IPO323 has a reduced set of effector genes (N=274) compared to Zt05 and Zt10 that encode  
244 approximately 30% more effector genes (N=417 and N=403, respectively, Figure S6B). Despite  
245 the high variability, the effector genes are mostly located on core chromosomes and none of the

246 five *Zymoseptoria* species have more than ten effector genes located on accessory  
247 chromosomes (Figure S1).

248 **The accessory genes of *Z. tritici* are shared with the closely related wild-grass infecting  
249 species**

250 To further characterize variation in gene content among the five *Zymoseptoria* species, we  
251 identified orthologous genes (i.e. orthogroups) from the gene predictions. We categorized 22341  
252 gene orthogroups identified in the seven *Zymoseptoria* genomes and in *C. beticola* according to  
253 their distribution among fungal genomes (Figure 4A). The core orthogroups, which are genes  
254 present in all eight genomes, represent around 30% of all orthogroups (N = 6698). The genus-  
255 specific orthogroups, shared between several *Zymoseptoria* spp. but not found in the *C. beticola*  
256 genome, represent 45% of the orthogroups (N = 9955; ranging from 2066 to 3212 per species).  
257 Among the genus-specific orthogroups, 1100 are found in all *Zymoseptoria* genomes (Figure  
258 4A), whereas all others show presence-absence polymorphisms within the genus. A total of  
259 2476 species-specific orthogroups (ranging from 552 to 1191 per species) are found only in  
260 individual species. Among the species-specific genes, 205 orthogroups (N<sub>genes</sub> = 414 to 562) are  
261 found in all three *Z. tritici* genomes while the isolate-specific genes in *Z. tritici* represent 391  
262 (Zt10) to 792 (IPO323) genes.

263 Comparing the three *Z. tritici* isolates independently from the other species, we observe  
264 extensive gene presence-absence polymorphisms between the three isolates: 1540 orthogroups  
265 are identified in only two strains and 2522 are found in only one (Figure 4B). The number of  
266 genes showing presence-absence variation is striking compared to the 10098 core genes in *Z.*  
267 *tritici* as these genes comprise almost 30% of all predicted genes. Interestingly, we show that the  
268 number of orthogroups detected as isolate-specific is much larger when the comparison includes  
269 only members of the same species than when the other species are included (1035, 849 and  
270 638 vs 792, 659 and 391 genes for IPO323, Zt05 and Zt10 respectively; Figures 4A and B). This  
271 indicates that a large part of the accessory gene content in *Z. tritici* is shared among the sister

272 species, and highlight the importance of including sister species when establishing core and  
273 accessory gene content.

274 Interestingly, we show that effectors are enriched among the *genus-specific* genes but not  
275 among the *species-specific* or *isolate-specific* gene categories (with the exception of *Z.*  
276 *ardabiliiae*). Fifty-six percent of effectors in *Z. ardabiliiae* and up to 78% of effectors in *Z.*  
277 *pseudotritici* are shared with at least one of the other five *Zymoseptoria* species (Figure 4C).  
278 Indeed, 427 effector orthogroups are found in at least two genomes. However, only 47 (10% of  
279 the total effector orthogroups N= 474) are found in all seven *Zymoseptoria* genomes. Among the  
280 effectors shared by *Z. tritici*, and at least one other *Zymoseptoria* species, 32% (N = 112 of 352)  
281 are present in all three *Z. tritici* isolates while 68% (N = 240 of 352) show presence-absence  
282 polymorphisms in at least one of the three isolates. These results indicate that the majority of  
283 these shared effectors is actually accessory (i.e. presence-absence polymorphism) in *Z. tritici*.

284 **Among *in planta* differentially expressed genes, species-specific are more expressed  
285 than core genes**

286 Finally, we addressed the functional relevance of accessory and orphan genes in *Z. tritici* by  
287 analyzing gene expression patterns. We used previously published transcriptome data of three  
288 *Z. tritici* isolates [30] and focused on gene expression of the above-defined categories (core  
289 genes, *genus-specific*, *species-specific*, and *isolate-specific*). We sorted *in planta* expression  
290 data into two different infection phases: the biotrophic phase and the necrotrophic phase, a  
291 separation supported by principal component analysis of normalized DESeq2 counts (Figure  
292 S7). We compared expression levels by mapping RNA-seq reads to the genomes of IPO323,  
293 Zt05 and Zt10, using normalized read mappings to transcript per million. We tested differences  
294 among gene categories using pairwise comparisons with a Kruskal-Wallis test (Figure 5).  
295 Overall, we find that gene expression of the *species-specific* and *isolate-specific* genes is  
296 significantly lower in IPO323 and Zt10, but not in Zt05 (Kruskal-Wallis p-value < 0.05). *Species-*  
297 *specific* and *isolate-specific* gene median expression ranges from 3.2 to 5.6 TPM in IPO323 and  
298 Zt10 while median expression of core genes is 12.1 and 10.9, respectively. The Zt05 expression

299 profile does not follow the same trend: the *core genes* are the lowest expressed gene category  
300 (8.9 median TPM), while *genus*-; *species*- and *isolate-specific* genes showed higher transcription  
301 levels (12.0; 14.4 and 13.5 median TPM respectively, Kruskal-Wallis p-value < 0.05).  
302 In contrast, we observe a significantly higher expression of the *species-specific* and *isolate-*  
303 *specific* genes for all three isolates (Table S2; Kruskal-Wallis p-value < 0.05) when comparing  
304 the expression of genes that are differentially expressed (DEGs; DESeq2 p-adjusted < 0.05)  
305 between the biotrophic and necrotrophic phases. *Species-specific* and *isolate-specific* DEGs are  
306 higher expressed *in planta* than the *core* and *genus-specific* genes (Figure 5B; Kruskal-Wallis p-  
307 value < 0.05). The expression pattern of DEGs with different levels of specificity present a  
308 consistent pattern in all three isolates (Table S2). Overall, this comparison reveals a potential  
309 functional relevance of accessory genes which are up-regulated during infection of *Z. tritici*.

310 **Discussion**

311 In this study we present a new resource of high-quality whole genome assemblies and gene  
312 annotations for the species *Z. ardabilliae*, *Z. brevis*, *Z. passerinii*, *Z. pseudotritici*, and two *Z. tritici*  
313 isolates. This new dataset provides a valuable resource for detailed analyses of genome  
314 architecture and evolutionary trajectories in this group of plant pathogens. Here, we conduct  
315 some first comparative analyses of genome architecture and show a considerable extent of  
316 variation in sequence composition during the recent evolution of *Zymoseptoria* lineages. We  
317 show that genome compartmentalization and accessory chromosomes represent shared  
318 ancestral traits among the pathogen species.

319

320 We identify extensive presence-absence variation of protein coding genes in genomes of five  
321 *Zymoseptoria* species consistent with the variable gene repertoire already reported for *Z. tritici*  
322 [28]. Furthermore, the different species, share a particular genomic architecture that comprises  
323 specific accessory genome compartments. In spite of this variation, we observe an overall  
324 conserved synteny of the core chromosomes. In the *Zymoseptoria* genomes, we observe gene-  
325 dense, actively transcribed and H3K4me2-enriched compartments covering most of the core  
326 chromosomes. These compartments are clearly distinguishable from gene-sparse, non-

327 transcribed and H3K4me2-deprived compartments. Based on previous analyses of accessory  
328 chromosomes in *Z. tritici*, we here consider this pattern as a specific hallmark of accessory  
329 genome compartments in the genus *Zymoseptoria* and not only in *Z. tritici* [6]. We hypothesize  
330 that these compartments likely represent accessory chromosomes in the different *Zymoseptoria*  
331 species.

332 We also identify accessory signatures in core chromosomes, including the previously described  
333 right arm of chromosome 7 [6]. Although this region has not been reported to share the same  
334 heavy pattern of presence-absence polymorphism as the accessory chromosomes, it is worth  
335 noting that a recent study identified a large deletion in chromosome 7 likely corresponding to this  
336 region in a single *Z. tritici* isolate originating from Yemen [37]. Here we show that this  
337 homologous region also exhibits accessory compartment hallmarks in the other *Zymoseptoria*  
338 species. A fusion between a core and an accessory chromosome occurred tens of thousands of  
339 years ago and prior to species divergence. The specific genomic and epigenetic features have  
340 remained stable through speciation and evolutionary time.

341  
342 In this study, we confirm previously reported genome comparisons showing that gene content in  
343 *Z. tritici* is highly variable [28]. We further extended the identification of orthologs throughout the  
344 whole *Zymoseptoria* genus. Thereby, we show that more than 25% of the genes identified as  
345 *isolate-specific* in a comparison including only *Z. tritici* isolates are actually shared with its wild-  
346 grass infecting sister species, proving that a large proportion of the accessory genome of *Z. tritici*  
347 is not specific to this species. Instead, the accessory genome content is shared among  
348 *Zymoseptoria* species. The proportion of accessory *Z. tritici* genes shared with other  
349 *Zymoseptoria* species was found to be the highest in the Iranian isolate, which is the only isolate  
350 sympatric with the four sister-species. A likely explanation for this observation would be inter-  
351 specific gene flow which would allow the different wild species to exchange genes with sympatric  
352 *Z. tritici* isolates. This new finding is consistent with recent findings from population genomic data  
353 studies revealing extensive introgression between *Zymoseptoria* species [38, 39]. It also opens

354 new perspectives for further analysis to understand how inter-specific gene flow has affected the  
355 evolution of the accessory genome of *Z. tritici*.

356

357 The genes with predicted functions and, in particular, functions related to pathogenicity are  
358 largely shared in *Zymoseptoria* genus. Although the lifestyles of the wild-grass infecting  
359 *Zymoseptoria* are poorly understood the species most likely share major features of their  
360 lifestyles. Thus, as expected, a similar CAZymes and BGC contents in all studied *Zymoseptoria*  
361 species was identified. Effector prediction is often used to better understand the adaptation of  
362 pathogens to their hosts [40]. However, in *Zymoseptoria*, the effectors are significantly enriched,  
363 not among the isolate- or even species-specific genes, but among the genes specific to the  
364 genus. If we exclude *Z. ardabiliiae*, the repertoire of effectors shared at the genus level  
365 represents three-quarters of all predicted effectors. This ratio suggests either that only a small  
366 number of effectors confer host specificity among the different *Zymoseptoria* species or that  
367 host-specificity is conferred not by presence-absence of these effectors but by regulation of their  
368 expression [30]. In the *Botrytis* genus (Dothideomycetes), sister species infecting different hosts  
369 share effectors with confirmed functions [41]. We hypothesize that the different specificity levels  
370 reflect functional differences in the effector repertoire of *Zymoseptoria*. Effectors conserved  
371 across the *Zymoseptoria* genus are core effectors, potentially targeting key plant defense  
372 mechanisms common to all of their hosts [42]. In contrast, effectors which are *species-specific* or  
373 *isolate-specific* might reflect host specificity and target specific pathogen recognition pathways  
374 [42]. This assumption is supported by the fact that only a fraction of the *genus-specific* effectors  
375 is actually shared among all *Zymoseptoria* species while the majority shows presence-absence  
376 polymorphisms. *Z. ardabiliiae* has been isolated from leaves of distantly related grass species in  
377 Iran, including *Lolium* spp., *Elymus repens*, and *Dactylis glomerata* and potentially resulting in a  
378 broader *species-specific* effector repertoire of *Z. ardabiliiae* compared to the other species [21].

379

380 Consistent with a previous study [28], we found that *Z. tritici* core genes are more expressed  
381 compared to accessory genes *in planta*. Core genes are more likely to hold essential functions

382 which could explain higher expression pattern during infection. Differentially expressed genes  
383 that are specifically induced during the course of the infection are very likely to have functions  
384 essential to pathogenicity of the fungus. Interestingly, here we show that within the differentially  
385 expressed genes between the biotrophic and the necrotrophic phases of infection, *isolate*- and  
386 *species-specific* genes have higher expression levels than core genes. These *isolate*- and  
387 *species-specific* genes could be functionally important and regulate functions linked to infection  
388 success in the biotrophic phase or to leaf colonization in the necrotrophic phase. Since these  
389 genes show presence-absence polymorphisms in the genus and in the *Z. tritici* species, they  
390 could represent a reservoir for possible adaptations to either host species, host cultivars or local  
391 environments.

392

### 393 **Conclusion**

394 We investigated the genomic architecture in a genus of plant pathogens, including the  
395 economically relevant wheat pathogen *Z. tritici*. Comparing genome content and genome  
396 structure, we identified a large shared effector repertoire characterized by inter- and intraspecies  
397 presence-absence polymorphisms. Major features of genomic, transcriptomic and epigenetic  
398 compartmentalization, distinguishing accessory and core compartments, were shared among  
399 wheat and wild-grass infecting *Zymoseptoria* species. We conclude that compartmentalization of  
400 genomes is an ancestral trait in the *Zymoseptoria* genus.

### 401 **Methods and Materials**

#### 402 **Fungal material, DNA extraction and sequencing**

403 Details regarding the individual *Zymoseptoria* isolates can be found in Table 1. For genomic data  
404 we used the three *Z. tritici* isolates IPO323 (reference), Zt05 and Zt10, one *Z. ardabiliiae* isolate  
405 (Za17), one *Z. brevis* isolate (Zb87), one *Z. passerinii* isolate (Zpa63), and the *Z. pseudotriticici*  
406 isolate (Zp13). For transcriptomic and epigenomic data we used *Z. tritici* Zt09 (IPO323  $\Delta$ Chr18) a  
407 derivate of the reference isolate IPO323 deleted with the chromosome 18 [31].

408 Long read assemblies of the *Z. tritici* isolates Zt05 and Zt10 were described and published  
409 previously [30]. For DNA extraction and long read sequencing cultures of *Z. pseudotritici*, *Z.*  
410 *ardabilliae*, *Z. brevis* and *Z. passerinii* were maintained in liquid YMS medium (4 g/L yeast  
411 extract, 4 g/L malt extract, 4 g/L sucrose) at 200 rpm and 18°C. DNA extraction was conducted  
412 as previously described [26]. PacBio SMRTbell libraries were prepared using DNA extracted  
413 from single cells based on a CTAB extraction protocol [43]. The libraries were size selected with  
414 an 8-kb cutoff on a BluePippin system (Sage Science).

415 After selection, the average fragment length was 15 kb. Sequencing of the isolates  
416 Za17, Zb87, and Zp13 was run on a PacBio RS II instrument at the Functional Genomics  
417 Center, Zurich, Switzerland. Sequencing of the Zpa63 isolate was performed at the Max Planck-  
418 Genome-Centre, Cologne, Germany.

419 **Genome assembly, and repeat and gene predictions**

420 For each isolate, we assembled the genome de novo using SMRT Analysis software v.5 (Pacific  
421 Bioscience) with two sets of parameters: default parameters and “fungal” parameters. We chose  
422 the best assemblies generated by comparison of all assembly statistics produced by the  
423 software Quast such as the number of finished contigs, the size of the assembly and the N50  
424 [44]. Summary statistics for each assembly can be found in Table 1. In order to exclude poor  
425 quality contigs from the raw assemblies, we filtered out the contigs with less than 1.5X and more  
426 than 2X median read coverage as these might be unreliable from lack of data or because they  
427 contain only repeated DNA. This filter removed a high number of contigs, i.e., between 58% and  
428 17% of contigs. Telomeric repeats (“CCCTAA”) were identified in the remaining contigs using  
429 bowtie2 to identify the number of fully assembled chromosomes or chromosomes arms based  
430 on the presence of more than six repeats at the contig extremities [45–47].  
431 We next used the REPET package to annotate the repeat regions of *Z. ardabilliae* Za17, *Z.*  
432 *brevis* Zb87, *Z. pseudotritici* Zp13, *Z. passerinii* Zpa63, and the three *Z. tritici* isolates  
433 IPO323, Zt5 and Zt10 (<https://urgi.versailles.inra.fr/Tools/REPET>; [48, 49]. For each genome, we

434 annotated the repetitive regions as follows: we first identified repetitive elements in each genome  
435 using TEdenovo following the developer's recommendations and default parameters. The library  
436 of identified consensus repeats was then used to annotate the respective genomes using  
437 TEannot with default parameters.

438 We used several different approaches to predict gene coordinates and leveraged the information  
439 contained in previously published RNA sequencing data to increase the quality of the prediction  
440 [22, 30, 32]. We used GeneMark-ES for the first prediction *ab initio* using the option “--fungus”  
441 [50]. We furthermore used previously obtained RNAseq data in two different ways: first by  
442 mapping the reads to the respective genomes and second by assembling them *de novo* into  
443 longer transcripts. For this, we first trimmed the reads using Trimmomatic [51], and then mapped  
444 them on the newly assembled genomes using hisat2 [47]. Next we used the BRAKER1 pipeline  
445 to predict genes for each genome using the fungus flag and based on the previously mapped  
446 reads [52]. BRAKER applies GeneMark-ET and Augustus to create the first step of gene  
447 predictions based on spliced alignments and to produce a final gene prediction based on the  
448 best prediction of the first set [53, 54]. In addition to the *ab initio* gene predictions, this produced  
449 a second set of predicted genes. Furthermore, the RNAseq reads were separately assembled  
450 into gene transcripts using Trinity [55]. These were aligned using PASA and EVidence Modeler  
451 to produce consensus gene models from the two independent predictions and the *de novo*  
452 assembled transcripts [56]. Gene counts, length and other summary statistics presented in Table  
453 S1 were obtained using GenomeTools [57] and customs scripts.

454 The predicted gene sequences were the basis for an evaluation of the completeness of the  
455 assembly and gene prediction by the program BUSCO v.3 [58]. We used this method with the  
456 lineage dataset *Pezizomycotina*. The predicted genes were also used to create a phylogeny with  
457 the online implementation of CVtree3, using kmer sizes of 6 and 7 as recommend for fungi [59].  
458 We generated a second tree with the whole assemblies, estimating a distance matrix using the  
459 andi software [60].

460 We predicted orthologs between the newly assembled genomes, the reference *Z. tritici* genome  
461 and the reference *Cercospora beticola* genome, a related Dothideomycete, which we used as

462 outgroup to identify genes with orthologs restricted to the *Zymoseptoria* genus [21]. For this, we  
463 used the software PoFF [35, 61] which takes into account synteny information in the analyses of  
464 similarity inferred by the program Proteinortho [35]. These orthogroups were used to visualize  
465 synteny between genomes using Circos [62].

466 The whole-genome assemblies were used to create a matrix distance with the software andi,  
467 from which we generated a tree [60]. A second tree was generated from the gene prediction with  
468 the online implementation of CVtree3 [59].

469 **Functional annotations**

470 We used several tools to predict the putative functions for the gene models. First, we used the  
471 eggnog-mapper which provide COG, GO and KEGG annotations [63]. The online resource  
472 dbCAN2 was run to identify carbohydrate-active enzymes (CAZymes) [64]. Finally, for each  
473 genome, we used Antismash v3 (fungal version) to detect biosynthetic gene clusters (Figure S1;  
474 [65]).

475 Additionally, we designed a pipeline to predict protein cell localization and to identify effector  
476 candidates. The pipeline for effector prediction is outlined in Figure S1 and includes the software  
477 DeepLoc [66], SignalP [67], TargetP [68], phobius [69] and TMHMM [70, 71], which predict the  
478 cellular location, the peptide signals and whether proteins are transmembrane. Effectors were  
479 identified with EffectorP v2 which uses both a new machine learning approach and more  
480 complete databases to improve effector prediction compared to the previous version [19]. The  
481 pipeline also includes software which are specifically targeted to annotate plant pathogenic  
482 functions, namely the program ApoplastP [72] and LOCALIZER [73]. We wrote wrappers scripts,  
483 which run the software and create consensus between the different prediction tools providing  
484 one command line from the user. These scripts are available at  
485 [https://gitlab.gwdg.de/alice.feurtey/genome\\_architecture\\_zymoseptoria](https://gitlab.gwdg.de/alice.feurtey/genome_architecture_zymoseptoria). Briefly, we gathered  
486 outputs of several software to predict the cellular location, transmembrane domain and secretion  
487 and created a consensus based on the different output to prevent the pitfalls of any one of these  
488 methods. From this consensus, we extracted the gene products predicted to be secreted and

489 without a transmembrane domain. The comparisons of genes functions repartition were done by  
490 combining predictions of COG categories, secondary metabolite genes with pathogenicity-  
491 related gene functional categories such as CAZymes and effector predictions.

492 **Gene expression analyses**

493 To update expression profiles on the new genome assemblies and new gene predictions of the  
494 three *Z. tritici* isolates, we used previously generated RNA-seq data from *in planta* and *in vitro*  
495 growth [30, 32]. The *in planta* RNAseq data was obtained from infected leaves at four different  
496 stages corresponding to early and late biotrophic (stage A and stage B) and necrotrophic (stage  
497 C and stage D) stages of the three *Z. tritici* isolates [30]. Strand-specific RNA-libraries were  
498 sequenced using Illumina HiSeq2500, with 100pb single-end reads for a total read number  
499 ranging from 89.5 to 147.5 million reads per sample. This data was previously analyzed [30],  
500 using gene predictions generated from an Illumina-based assembly [22]. The reads were here  
501 mapped on the new assemblies of Zt5 and Zt10 and the reference genome of IPO323 after  
502 trimming. We used the DESeq2 R package to determine differential gene expression during *in*  
503 *planta* infection, considering only two infection stages; biotrophic and necrotrophic [74]. Gene  
504 expression was assessed as Transcript per Million (TPM). Briefly, TPM is calculated by  
505 normalizing read counts with coding region length resulting in the number of reads per kilobase  
506 (RPK). RPK total counts per sample are then divided by 1 million to generate a “per million”  
507 scaling factor. We calculated the coding region length of each gene with GenomicFeatures R  
508 package using the function called “exonsBy” [75]. For gene expression analyses, we further  
509 filtered our gene predictions to remove any predicted transposases and other TE-related  
510 annotations based on the Eggnog mapper annotations.

511 **ChIP-sequencing and data analysis**

512 *Z. ardabilliae* (Za17) and *Z. pseudotritici* (Zp13) cells were grown in liquid YMS medium for two  
513 days at 18°C until an OD<sub>600</sub> of ~ 1 was reached. Chromatin immunoprecipitation and library  
514 preparation were performed as previously described [76]. We sequenced two biological and two  
515 technical replicates per isolate and used antibodies against the euchromatin histone mark

516 H3K4me2 (#07–030, Merck Millipore). Sequencing was performed at the OSU Center for  
517 Genome Research and Biocomputing (Oregon State University, Corvallis, USA) on an Illumina  
518 HiSeq2000 to obtain 50-nt reads. The data was quality-filtered using the FastX toolkit  
519 ([http://hannonlab.cshl.edu/fastx\\_toolkit/](http://hannonlab.cshl.edu/fastx_toolkit/)), mapping was performed using bowtie2 [77] and peaks  
520 were called using HOMER [78]. Peaks were called individually for each replicate, but only peaks  
521 that were detected in all replicates were considered and merged for further analysis. Merging of  
522 peaks and genome wide sequence coverage with enriched regions was assessed using  
523 bedtools [46].

524 **Data availability**

525 The assembled genomes can be found at 10.5281/zenodo.3568213. The gene annotations are  
526 deposited at 10.5281/zenodo.3568213. The functional annotation pipeline, additional scripts and  
527 command lines used to create the results presented in this manuscript can be found at  
528 [https://gitlab.gwdg.de/alice.feurtey/genome\\_architecture\\_zymoseptoria](https://gitlab.gwdg.de/alice.feurtey/genome_architecture_zymoseptoria).

529 **Ethics approval and consent to participate**

530 Not applicable.

531 **Consent for publication**

532 Not applicable.

533 **Availability of data and materials**

534 All the data supporting the findings of this study are openly available at  
535 10.5281/zenodo.3568213.

536 **Competing interests**

537 The authors declare that they have no competing interests.

538 **Funding and Acknowledgements**

539 CL is funded by the Institut national de la recherche agronomique (INRA) in the framework of a  
540 “Contrat Jeune Scientifique” and by the Labex ARBRE (Lab of Excellence ARBRE). Genome  
541 research in the group of EHS is funded by the DFG Priority Program SPP1819 and the

542 Canadian Institute for Advanced Research (CIFAR). AF is funded by by the DFG Priority  
543 Program SPP1819.

544 **Authors' contributions**

545 AF, CL and MM performed data and results analyses. EHS, AF and CL contributed to the design  
546 and implementation of the research. AF, CL, CE and DC performed genome assemblies. MH,  
547 JH, MM, MF and KS performed the experimental procedures. All authors contributed to the  
548 writing of the manuscript.

549 **References**

- 550 1. Cook DE, Mesarich CH, Thomma BPHJ. Understanding plant immunity as a surveillance  
551 system to detect invasion. *Annu Rev Phytopathol.* 2015;53:541–63.
- 552 2. Rouxel T, Grandaubert J, Hane JK, Hoede C, van de Wouw AP, Couloux A, et al. Effector  
553 diversification within compartments of the *Leptosphaeria maculans* genome affected by Repeat-  
554 Induced Point mutations. *Nat Commun.* 2011;2:202.
- 555 3. Dong S, Raffaele S, Kamoun S. The two-speed genomes of filamentous pathogens: waltz  
556 with plants. *Curr Opin Genet Dev.* 2015;35:57–65. doi:10.1016/j.gde.2015.09.001.
- 557 4. Todd RT, Wikoff TD, Forche A, Selmecki A. Genome plasticity in *Candida albicans* is driven  
558 by long repeat sequences. *eLife.* 2019;8. doi:10.7554/eLife.45954.
- 559 5. Mehrabi R, Mirzadi Gohari A, Kema GHJ. Karyotype Variability in Plant-Pathogenic Fungi.  
560 *Annu Rev Phytopathol.* 2017;55:483–503. doi:10.1146/annurev-phyto-080615-095928.
- 561 6. Schotanus K, Soyer JL, Connolly LR, Grandaubert J, Happel P, Smith KM, et al. Histone  
562 modifications rather than the novel regional centromeres of *Zymoseptoria tritici* distinguish core  
563 and accessory chromosomes. *Epigenetics Chromatin.* 2015;8:41. doi:10.1186/s13072-015-  
564 0033-5.
- 565 7. Fokkens L, Shahi S, Connolly LR, Stam R, Schmidt SM, Smith KM, et al. The multi-speed  
566 genome of &lt;em&gt;*Fusarium oxysporum*&lt;/em&gt; reveals association of histone  
567 modifications with sequence divergence and footprints of past horizontal chromosome transfer  
568 events. *bioRxiv.* 2018;:465070.

569 8. Miao VP, Covert SF, Vanetrent HD. A Fungal Gene for Antibiotic Resistance on a  
570 Dispensable ("B") Chromosome. *Science* (80-). 1991;254. doi:10.1126/science.1763326.

571 9. Temporini E, VanEtten H. An analysis of the phylogenetic distribution of the pea pathogenicity  
572 genes of *Nectria haematococca* MPVI supports the hypothesis of their origin by horizontal  
573 transfer and uncovers a potentially new pathogen of garden pea: *Neocosmospora boniensis*.  
574 *Curr Genet.* 2004;46:29–36. doi:10.1007/s00294-004-0506-8.

575 10. Ma L-J, van der Does HC, Borkovich KA, Coleman JJ, Daboussi M-JM-J, Di Pietro A, et al.  
576 Comparative genomics reveals mobile pathogenicity chromosomes in *Fusarium*. *Nature*.  
577 2010;464:367–73.

578 11. Balesdent M-H, Fudal I, Ollivier B, Bally P, Grandaubert J, Eber F, et al. The dispensable  
579 chromosome of *Leptosphaeria maculans* shelters an effector gene conferring avirulence towards  
580 *Brassica rapa*. *New Phytol.* 2013;198:887–98.

581 12. van der Does HC, Rep M. Adaptation to the Host Environment by Plant-Pathogenic Fungi.  
582 *Annu Rev Phytopathol.* 2017;55:427–50.

583 13. Lorrain C, Petre B, Duplessis S. Show me the way: rust effector targets in heterologous plant  
584 systems. *Curr Opin Microbiol.* 2018;46:19–25.

585 14. Toruño TY, Stergiopoulos I, Coaker G. Plant-Pathogen Effectors: Cellular Probes Interfering  
586 with Plant Defenses in Spatial and Temporal Manners. *Annu Rev Phytopathol.* 2016;54:419–41.  
587 doi:10.1146/annurev-phyto-080615-100204.

588 15. Zhao Z, Liu H, Wang C, Xu J-R. Comparative analysis of fungal genomes reveals different  
589 plant cell wall degrading capacity in fungi. *BMC Genomics.* 2013;14:274. doi:10.1186/1471-  
590 2164-14-274.

591 16. Lo Presti L, Lanver D, Schweizer G, Tanaka S, Liang L, Tollot M, et al. Fungal Effectors and  
592 Plant Susceptibility. *Annu Rev Plant Biol.* 2015;66:513–45. doi:10.1146/annurev-arplant-043014-  
593 114623.

594 17. Snelders NC, Kettles GJ, Rudd JJ, Thomma BPHJ. Plant pathogen effector proteins as  
595 manipulators of host microbiomes? *Mol Plant Pathol.* 2018;19:257–9.

596 18. Shi-Kunne X, Jové R de P, Depotter JRL, Ebert MK, Seidl MF, Thomma BPHJ. In silico

597 prediction and characterisation of secondary metabolite clusters in the plant pathogenic fungus  
598 *Verticillium dahliae*. FEMS Microbiol Lett. 2019;366.

599 19. Sperschneider J, Dodds PN, Gardiner DM, Singh KB, Taylor JM. Improved prediction of  
600 fungal effector proteins from secretomes with EffectorP 2.0. Mol Plant Pathol. 2018;19:2094–  
601 110. doi:10.1111/mpp.12682.

602 20. Stukenbrock EH, Banke S, Javan-Nikkhah M, McDonald BA. Origin and domestication of the  
603 fungal wheat pathogen *Mycosphaerella graminicola* via sympatric speciation. Mol Biol Evol.  
604 2007;24:398–411.

605 21. Stukenbrock EH, Quaedvlieg W, Javan-Nikkhah M, Zala M, Crous PW, McDonald BA.  
606 *Zymoseptoria ardabilliae* and *Z. pseudotritici*, two progenitor species of the septoria tritici leaf  
607 blotch fungus *Z. tritici* (synonym: *Mycosphaerella graminicola*). Mycologia. 2012;104:1397–407.  
608 doi:10.3852/11-374.

609 22. Grandaubert J, Bhattacharyya A, Stukenbrock EH. RNA-seq-Based Gene Annotation and  
610 Comparative Genomics of Four Fungal Grass Pathogens in the Genus *Zymoseptoria* Identify  
611 Novel Orphan Genes and Species-Specific Invasions of Transposable Elements. G3 (Bethesda).  
612 2015;5:1323–33. doi:10.1534/g3.115.017731.

613 23. Goodwin SB, Ben M'Barek S, Dhillon B, Wittenberg AHJ, Crane CF, Hane JK, et al. Finished  
614 Genome of the Fungal Wheat Pathogen *Mycosphaerella graminicola* Reveals Dispensome  
615 Structure, Chromosome Plasticity, and Stealth Pathogenesis. PLoS Genet. 2011;7:e1002070.  
616 doi:10.1371/journal.pgen.1002070.

617 24. Habig M, Quade J, Stukenbrock EH. Forward Genetics Approach Reveals Host Genotype-  
618 Dependent Importance of Accessory Chromosomes in the Fungal Wheat Pathogen  
619 *Zymoseptoria tritici*. MBio. 2017;8:e01919-17.

620 25. Habig M, Kema G, Holtgrewe Stukenbrock E. Meiotic drive of female-inherited  
621 supernumerary chromosomes in a pathogenic fungus. Elife. 2018.

622 26. Möller M, Habig M, Freitag M, Stukenbrock EH. Extraordinary Genome Instability and  
623 Widespread Chromosome Rearrangements During Vegetative Growth. Genetics.  
624 2018;210:517–29. doi:10.1534/genetics.118.301050.

625 27. Fouché S, Plissonneau C, McDonald BA, Croll D. Meiosis Leads to Pervasive Copy-Number  
626 Variation and Distorted Inheritance of Accessory Chromosomes of the Wheat Pathogen  
627 *Zymoseptoria tritici*. *Genome Biol Evol*. 2018;10:1416–29. doi:10.1093/gbe/evy100.

628 28. Plissonneau C, Hartmann FE, Croll D. Pangenome analyses of the wheat pathogen  
629 *Zymoseptoria tritici* reveal the structural basis of a highly plastic eukaryotic genome. *BMC Biol*.  
630 2018;16:5. doi:10.1186/s12915-017-0457-4.

631 29. Hartmann FE, McDonald BA, Croll D. Genome-wide evidence for divergent selection  
632 between populations of a major agricultural pathogen. *Mol Ecol*. 2018;27:2725–41.

633 30. Haueisen J, Möller M, Eschenbrenner CJ, Grandaubert J, Seybold H, Adamiak H, et al.  
634 Highly flexible infection programs in a specialized wheat pathogen. *Ecol Evol*. 2018.  
635 doi:10.1002/ece3.4724.

636 31. Kellner R, Bhattacharyya A, Poppe S, Hsu TY, Brem RB, Stukenbrock EH. Expression  
637 profiling of the wheat pathogen *Zymoseptoria tritici* reveals genomic patterns of transcription and  
638 host-specific regulatory programs. *Genome Biol Evol*. 2014;6:1353–65. doi:10.1093/gbe/evu101.

639 32. Möller M, Schotanus K, Soyer JL, Haueisen J, Happ K, Stralucke M, et al. Destabilization of  
640 chromosome structure by histone H3 lysine 27 methylation. *PLOS Genet*. 2019;15:e1008093.  
641 doi:10.1371/journal.pgen.1008093.

642 33. Plissonneau C, Stürchler A, Croll D. The Evolution of Orphan Regions in Genomes of a  
643 Fungal Pathogen of Wheat. *MBio*. 2016;7:e01231-16.

644 34. Vaghefi N, Kikkert JR, Bolton MD, Hanson LE, Secor GA, Pethybridge SJ. De novo genome  
645 assembly of *Cercospora beticola* for microsatellite marker development and validation. *Fungal*  
646 *Ecol*. 2017;26:125–34.

647 35. Lechner M, Findeiß S, Steiner L, Marz M, Stadler PF, Prohaska SJ. Proteinortho: Detection  
648 of (Co-)orthologs in large-scale analysis. *BMC Bioinformatics*. 2011;12:124. doi:10.1186/1471-  
649 2105-12-124.

650 36. Lorrain C, Hecker A, Duplessis S. Effector-Mining in the Poplar Rust Fungus *Melampsora*  
651 *larici-populina* Secretome . *Frontiers in Plant Science* . 2015;6:1051.

652 37. Badet T, Oggendorf U, Abraham L, McDonald BA, Croll D. A 19-isolate reference-quality

653 global pangenome for the fungal wheat pathogen *Zymoseptoria tritici*. bioRxiv. 2019;:803098.  
654 doi:10.1101/803098.

655 38. Feurtey A, Stevens DM, Stephan W, Stukenbrock EH. Interspecific Gene Exchange  
656 Introduces High Genetic Variability in Crop Pathogen. *Genome Biol Evol*. 2019;11:3095–105.  
657 doi:10.1093/gbe/evz224.

658 39. Wu B, Macielog AI, Hao W. Origin and Spread of Spliceosomal Introns: Insights from the  
659 Fungal Clade *Zymoseptoria*. *Genome Biol Evol*. 2017;9:2658–67. doi:10.1093/gbe/evx211.

660 40. Schulze-Lefert P, Panstruga R. A molecular evolutionary concept connecting nonhost  
661 resistance, pathogen host range, and pathogen speciation. *Trends Plant Sci*. 2011;16:117–25.

662 41. Valero-Jiménez CA, Veloso J, Staats M, van Kan JAL. Comparative genomics of plant  
663 pathogenic *Botrytis* species with distinct host specificity. *BMC Genomics*. 2019;20:203.

664 42. Thines M. An evolutionary framework for host shifts – jumping ships for survival. *New Phytol*.  
665 2019;:605–17.

666 43. Allen GC, Flores-Vergara MA, Krasynanski S, Kumar S, Thompson WF. A modified protocol  
667 for rapid DNA isolation from plant tissues using cetyltrimethylammonium bromide. *Nat Protoc*.  
668 2006;1:2320–5.

669 44. Gurevich A, Saveliev V, Vyahhi N, Tesler G. QUAST: quality assessment tool for genome  
670 assemblies. *Bioinformatics*. 2013;29:1072–5. doi:10.1093/bioinformatics/btt086.

671 45. Fulnecková J, Sevcíková T, Fajkus J, Lukesová A, Lukes M, Vlcek C, et al. A broad  
672 phylogenetic survey unveils the diversity and evolution of telomeres in eukaryotes. *Genome Biol  
673 Evol*. 2013;5:468–83. doi:10.1093/gbe/evt019.

674 46. Quinlan AR, Hall IM. BEDTools: a flexible suite of utilities for comparing genomic features.  
675 *Bioinformatics*. 2010;26:841–2. doi:10.1093/bioinformatics/btq033.

676 47. Kim D, Langmead B, Salzberg SL. HISAT: a fast spliced aligner with low memory  
677 requirements. *Nat Methods*. 2015;12:357–60. doi:10.1038/nmeth.3317.

678 48. Flutre T, Duprat E, Feuillet C, Quesneville H. Considering Transposable Element  
679 Diversification in De Novo Annotation Approaches. *PLoS One*. 2011;6:e16526.  
680 doi:10.1371/journal.pone.0016526.

681 49. Quesneville H, Bergman CM, Andrieu O, Autard D, Nouaud D, Ashburner M, et al.  
682 Combined Evidence Annotation of Transposable Elements in Genome Sequences. PLoS  
683 Comput Biol. 2005;1:e22. doi:10.1371/journal.pcbi.0010022.  
684 50. Ter-Hovhannisyan V, Lomsadze A, Chernoff YO, Borodovsky M. Gene prediction in novel  
685 fungal genomes using an ab initio algorithm with unsupervised training. Genome Res.  
686 2008;18:1979–90. doi:10.1101/gr.081612.108.  
687 51. Bolger AM, Lohse M, Usadel B. Trimmomatic: a flexible trimmer for Illumina sequence data.  
688 Bioinformatics. 2014;30:2114–20. doi:10.1093/bioinformatics/btu170.  
689 52. Hoff KJ, Lange S, Lomsadze A, Borodovsky M, Stanke M. BRAKER1: Unsupervised RNA-  
690 Seq-Based Genome Annotation with GeneMark-ET and AUGUSTUS: Table 1. Bioinformatics.  
691 2016;32:767–9. doi:10.1093/bioinformatics/btv661.  
692 53. Stanke M, Diekhans M, Baertsch R, Haussler D. Using native and syntenically mapped  
693 cDNA alignments to improve de novo gene finding. Bioinformatics. 2008;24:637–44.  
694 doi:10.1093/bioinformatics/btn013.  
695 54. Lomsadze A, Burns PD, Borodovsky M. Integration of mapped RNA-Seq reads into  
696 automatic training of eukaryotic gene finding algorithm. Nucleic Acids Res. 2014;42:e119–e119.  
697 doi:10.1093/nar/gku557.  
698 55. Grabherr MG, Haas BJ, Yassour M, Levin JZ, Thompson DA, Amit I, et al. Full-length  
699 transcriptome assembly from RNA-Seq data without a reference genome. Nat Biotechnol.  
700 2011;29:644–52. doi:10.1038/nbt.1883.  
701 56. Haas BJ, Salzberg SL, Zhu W, Pertea M, Allen JE, Orvis J, et al. Automated eukaryotic gene  
702 structure annotation using EVidenceModeler and the Program to Assemble Spliced Alignments.  
703 Genome Biol. 2008;9:R7. doi:10.1186/gb-2008-9-1-r7.  
704 57. Gremme G, Steinbiss S, Kurtz S. GenomeTools: A Comprehensive Software Library for  
705 Efficient Processing of Structured Genome Annotations. IEEE/ACM Trans Comput Biol  
706 Bioinforma. 2013;10:645–56. doi:10.1109/TCBB.2013.68.  
707 58. Waterhouse RM, Seppey M, Simão FA, Manni M, Ioannidis P, Klioutchnikov G, et al.  
708 BUSCO Applications from Quality Assessments to Gene Prediction and Phylogenomics. Mol

709 Biol Evol. 2018;35:543–8. doi:10.1093/molbev/msx319.

710 59. Zuo G, Hao B. CVTree3 Web Server for Whole-genome-based and Alignment-free

711 Prokaryotic Phylogeny and Taxonomy. *Genomics Proteomics Bioinformatics*. 2015;13:321–31.

712 doi:10.1016/J.GPB.2015.08.004.

713 60. Haubold B, Klötzl F, Pfaffelhuber P. andi: Fast and accurate estimation of evolutionary

714 distances between closely related genomes. *Bioinformatics*. 2015;31:1169–75.

715 doi:10.1093/bioinformatics/btu815.

716 61. Lechner M, Hernandez-Rosales M, Doerr D, Wieseke N, Thévenin A, Stoye J, et al.

717 Orthology detection combining clustering and synteny for very large datasets. *PLoS One*.

718 2014;9:e105015. doi:10.1371/journal.pone.0105015.

719 62. Krzywinski M, Schein J, Birol I, Connors J, Gascoyne R, Horsman D, et al. Circos: an

720 information aesthetic for comparative genomics. *Genome Res*. 2009;19:1639–45.

721 63. Huerta-Cepas J, Forlund K, Coelho LP, Szklarczyk D, Jensen LJ, von Mering C, et al. Fast

722 Genome-Wide Functional Annotation through Orthology Assignment by eggNOG-Mapper. *Mol*

723 *Biol Evol*. 2017;34:2115–22. doi:10.1093/molbev/msx148.

724 64. Zhang H, Yohe T, Huang L, Entwistle S, Wu P, Yang Z, et al. dbCAN2: a meta server for

725 automated carbohydrate-active enzyme annotation. *Nucleic Acids Res*. 2018;46:W95–101.

726 doi:10.1093/nar/gky418.

727 65. Weber T, Blin K, Duddela S, Krug D, Kim HU, Brucolieri R, et al. antiSMASH 3.0—a

728 comprehensive resource for the genome mining of biosynthetic gene clusters. *Nucleic Acids*

729 *Res*. 2015;43:W237–43. doi:10.1093/nar/gkv437.

730 66. Almagro Armenteros JJ, Sønderby CK, Sønderby SK, Nielsen H, Winther O. DeepLoc:

731 prediction of protein subcellular localization using deep learning. *Bioinformatics*. 2017;33:3387–

732 95. doi:10.1093/bioinformatics/btx431.

733 67. Petersen TN, Brunak S, von Heijne G, Nielsen H. SignalP 4.0: discriminating signal peptides

734 from transmembrane regions. *Nat Methods*. 2011;8:785–6. doi:10.1038/nmeth.1701.

735 68. Emanuelsson O, Nielsen H, Brunak S, von Heijne G. Predicting Subcellular Localization of

736 Proteins Based on their N-terminal Amino Acid Sequence. *J Mol Biol*. 2000;300:1005–16.

737 doi:10.1006/jmbi.2000.3903.

738 69. Käll L, Krogh A, Sonnhammer EL. A Combined Transmembrane Topology and Signal

739 Peptide Prediction Method. *J Mol Biol.* 2004;338:1027–36. doi:10.1016/j.jmb.2004.03.016.

740 70. Krogh A, Larsson B, von Heijne G, Sonnhammer EL. Predicting transmembrane protein

741 topology with a hidden markov model: application to complete genomes<sup>11</sup>Edited by F. Cohen. *J*

742 *Mol Biol.* 2001;305:567–80. doi:10.1006/jmbi.2000.4315.

743 71. Sonnhammer EL, von Heijne G, Krogh A. A hidden Markov model for predicting

744 transmembrane helices in protein sequences. *Proceedings Int Conf Intell Syst Mol Biol.*

745 1998;6:175–82. <http://www.ncbi.nlm.nih.gov/pubmed/9783223>. Accessed 26 Jun 2019.

746 72. Sperschneider J, Dodds PN, Singh KB, Taylor JM. ApoplastP<sup>□</sup>: prediction of effectors and

747 plant proteins in the apoplast using machine learning. *New Phytol.* 2018;217:1764–78.

748 doi:10.1111/nph.14946.

749 73. Sperschneider J, Catanzariti A-M, DeBoer K, Petre B, Gardiner DM, Singh KB, et al.

750 LOCALIZER: subcellular localization prediction of both plant and effector proteins in the plant

751 cell. *Sci Rep.* 2017;7:44598. doi:10.1038/srep44598.

752 74. Love MI, Huber W, Anders S. Moderated estimation of fold change and dispersion for RNA-

753 seq data with DESeq2. *Genome Biol.* 2014;15:550. doi:10.1186/s13059-014-0550-8.

754 75. Lawrence M, Huber W, Pagès H, Aboyoun P, Carlson M, Gentleman R, et al. Software for

755 Computing and Annotating Genomic Ranges. *PLoS Comput Biol.* 2013;9:e1003118.

756 doi:10.1371/journal.pcbi.1003118.

757 76. Soyer JL, Möller M, Schotanus K, Connolly LR, Galazka JM, Freitag M, et al. Chromatin

758 analyses of *Zymoseptoria tritici*: Methods for chromatin immunoprecipitation followed by high-

759 throughput sequencing (ChIP-seq). *Fungal Genet Biol.* 2015;79:63–70.

760 doi:10.1016/j.fgb.2015.03.006.

761 77. Langmead B, Salzberg SL. Fast gapped-read alignment with Bowtie 2. *Nat Methods.*

762 2012;9:357–9. doi:10.1038/nmeth.1923.

763 78. Heinz S, Benner C, Spann N, Bertolino E, Lin YC, Laslo P, et al. Simple combinations of

764 lineage-determining transcription factors prime cis-regulatory elements required for macrophage

765 and B cell identities. Mol Cell. 2010;38:576–89. doi:10.1016/j.molcel.2010.05.004.

766

767 Table 1: Metrics of genome assemblies and annotation

Species	<i>Zymoseptoria tritici</i>		<i>Zymoseptoria pseudotritici</i>	<i>Zymoseptoria brevis</i>	<i>Zymoseptoria ardabiliiae</i>	<i>Zymoseptoria passerinii</i>
<b>Isolate</b>	Zt05	Zt10	Zp13	Zb87	Za17	Zpa63
<b>Origin</b>	Denmark	Iran, Ilam province	Iran, Ardabil province	Iran	Ardabil province	USA
<b>Host</b>	<i>Triticum aestivum</i>	<i>Triticum aestivum</i>	<i>Dactylis glomerata</i>	<i>Phalaris paradoxa</i>	<i>Lolium perenne</i>	<i>Hordeum vulgare</i>
<b>Year (of isolation)</b>	2004	2001	2004		2004	
<b>Contig number</b>	30	19	42	29	50	103
<b>Total length (bp)</b>	41240984	39248105	40312446	41586671	38100668	41398787
<b>Mean contig size (bp)</b>	1374699	2065690	59820	1434023	762013	401930
<b>N50</b>	2454671	2925395	2115121	2744794	1156695	737698
<b>L50</b>	6	5	7	7	11	18
<b>Contigs with telomeric repeats on both ends</b>	12	19	5	9	0	0
<b>Number of genes</b>	12386	11991	11661	11480	11463	10528
<b>Repeat content (%)</b>	19.9	16.5	20.8	29.2	18.2	31.4

## Figure Legends

**Figure 1: Whole-genome phylogeny of *Zymoseptoria* spp. and basic statistics for the assemblies and gene predictions.** Tree based on the distance matrix generated from the whole-genome assemblies using the software andi (Haubold et al. 2015). The bar plots represent the number of genes coding for secreted proteins (pink) and non-secreted proteins (grey) for each genome.

**Figure 2: Intra- and inter-species synteny conservation in *Zymoseptoria* genus.** A) Intra-species synteny between the reference genome of *Z. tritici* and the genome of the Iranian *Z. tritici* isolate Zt10. Each color represents a different chromosome as defined in the reference *Z. tritici* genome, except for accessory chromosomes, which are in grey. The links represent orthologous genes. B) Inter-species synteny between the reference genome of *Z. tritici* and the genome of *Z. brevis*. The arrows represent the large-scale inversions identified between the genomes of these two species.

**Figure 3: Genome architecture of the reference genome *Z. tritici* IPO323 (A) and *Z. pseudotritici* Zp13 (B).** The segments constituting the first circle represents the chromosomes of IPO323 (A) and contigs of Zp13 (B) ordered according to chromosome numbers of the reference genome. Tracks from the outside to the inside are heatmaps representing respectively: gene density along chromosomes/contigs; gene expression in vitro (TPM); H3K4me2 levels in vitro and species-specific gene density. The arrows indicate the location of the region on chromosome 7 (and the corresponding syntenic region in *Z. pseudotritici*) displaying accessory-like genomic and regulatory hallmarks.

**Figure 4: Orthogroups and functional gene categories in *Zymoseptoria* spp. genomes.** A) Orthogroups shared by the reference *Z. tritici* genome, our new *Zymoseptoria* assemblies and the outgroup genome of *C. beticola*. Only intersects higher than 100 are displayed on the upset plot. The doughnut plot summarizes the number of orthologs grouped by larger categories: specific to some isolates, to a species or shared by all. The colored bars under the upset plot link each intersect to its corresponding category in the doughnut plot. B) Venn diagram representing the genes shared by the three isolates of *Z. tritici*. C) The only gene category found to be overrepresented in any of the specificity categories - other than unknown function genes - are effectors. Effectors genes are overrepresented in the genus-specific genes and in *Z. ardabilliae* specific genes (\*\* represent Fisher exact test p-value < 0.05).

**Figure 5: Expression of genes belonging to different specificity levels in the *Zymoseptoria* pangenome.** The boxplots represent the expression levels in both biotrophic and necrotrophic phase in transcript per million (TPM) for A) the whole transcriptome of *Z. tritici* isolates and B) in planta differentially expressed genes identified by DESeq2. Comparisons are performed by Krustal-Wallis test, different letters represent p-value < 0.05.

## Supplementary Tables

Table S1: Summary statistics from gene predictions generated in this study.

Table S2: Summary of gene expression in *Z. tritici* isolates during infection stages

Table S3: Enrichment of species-specific and isolate-specific genes per chromosome/contig

## Supplementary Figure Legends

**Figure S1:** Plant-associated genes compartmentalization along the chromosomes. The first track represents core (dark grey) and accessory (light grey) chromosomes/contigs. Fully assembled contigs are marked by the presence of telomeric repeats (orange). Circles from outside to inside represent the position of: effector genes (blue), biosynthetic gene clusters (BGC, green) and CAZymes (yellow), respectively.

**Figure S2:** A) Intra-species synteny between the reference genome of *Z. tritici* and the genome of the *Z. tritici* isolate Zt05. Each color represents a different chromosome as based on the reference *Z. tritici* genome, except for accessory chromosomes, which are in grey. The connecting lines represent orthologs between each genome. The track between the chromosomes and connecting lines are predicted effectors. B) Inter-species synteny between reference genome of *Z. tritici* and *Z. pseudotritici*. The arrows represent the large-scale inversions identified between the genomes of these two species.

**Figure S3:** Inter-species synteny between genomes of *Z. pseudotritici* (dark grey) and *Z. brevis* (blue). The arrows indicate the contigs affected by the large-scale inversions identified between *Z. tritici* and both *Z. pseudotritici* and *Z. brevis*.

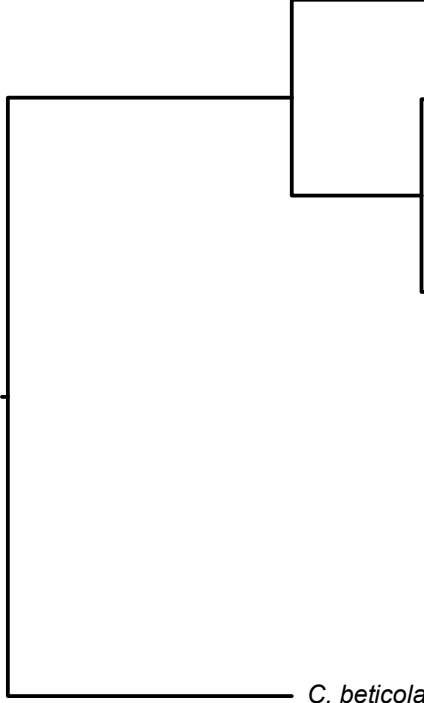
**Figure S4:** Genome architecture in A) *Z. tritici* Zt05, B) *Z. tritici* Zt10. C) *Z. brevis* Zb87 and D) *Z. ardabiliiae* Za17. Circles from the outside to the inside represent respectively: gene density along chromosomes/contigs; gene expression in vitro (TPM); H3K4me2 distribution in vitro (only for Za17) and species-specific gene density

**Figure S5:** Simplified diagram of the pipeline used to predict the functions and subcellular localization of gene model products.

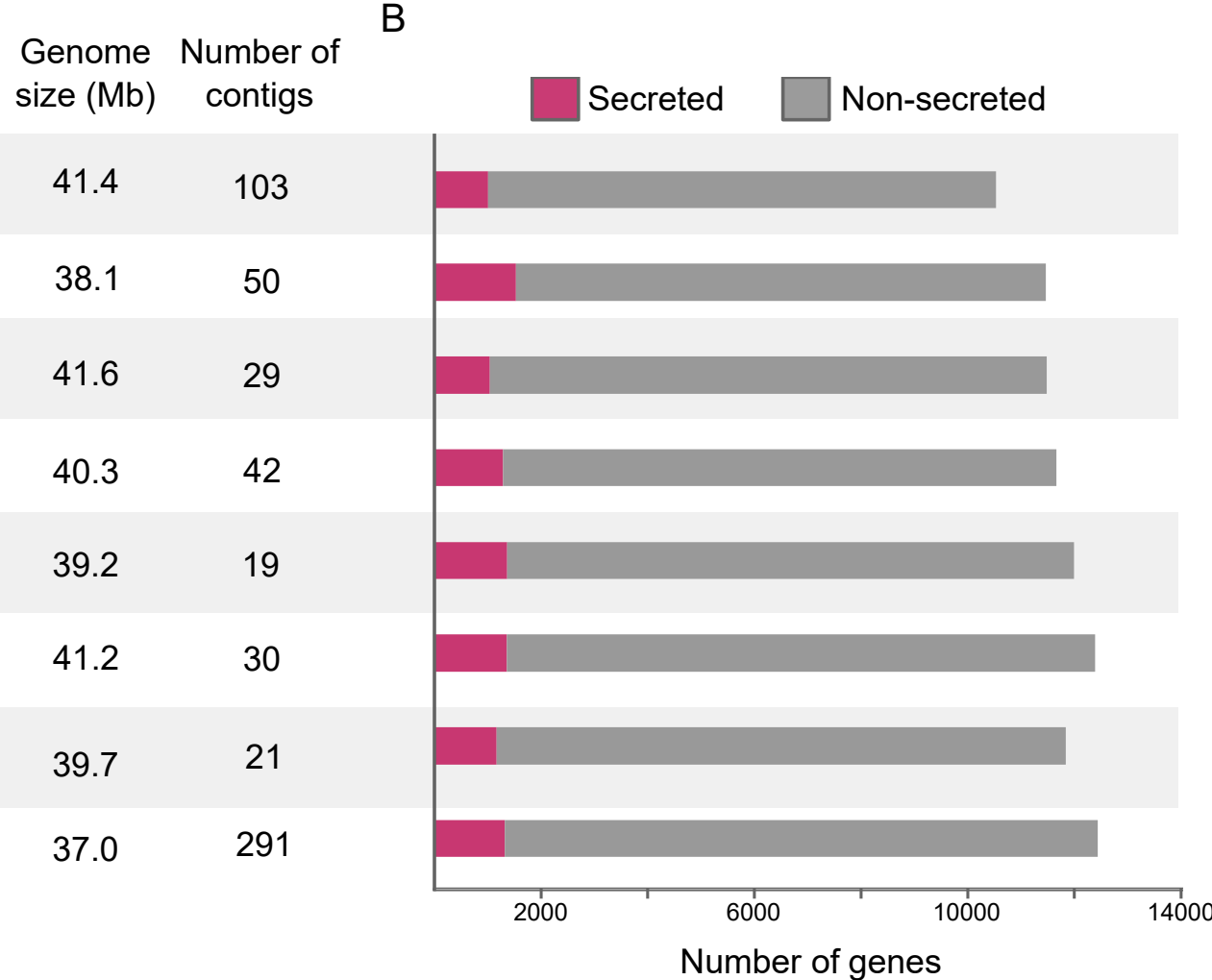
**Figure S6:** Functional gene categories in *Zymoseptoria spp.* genomes. A) The number of genes in Eggmapper COG categories in addition to Effectors and CAZymes. B) Pathogenicity-related genes of interest: secreted proteins, effectors, secreted CAZymes and non-secreted CAZymes. C) Subcellular localization of predicted gene products.

**Figure S7:** Principal component analysis of DESeq2 rlog transformed expression data.

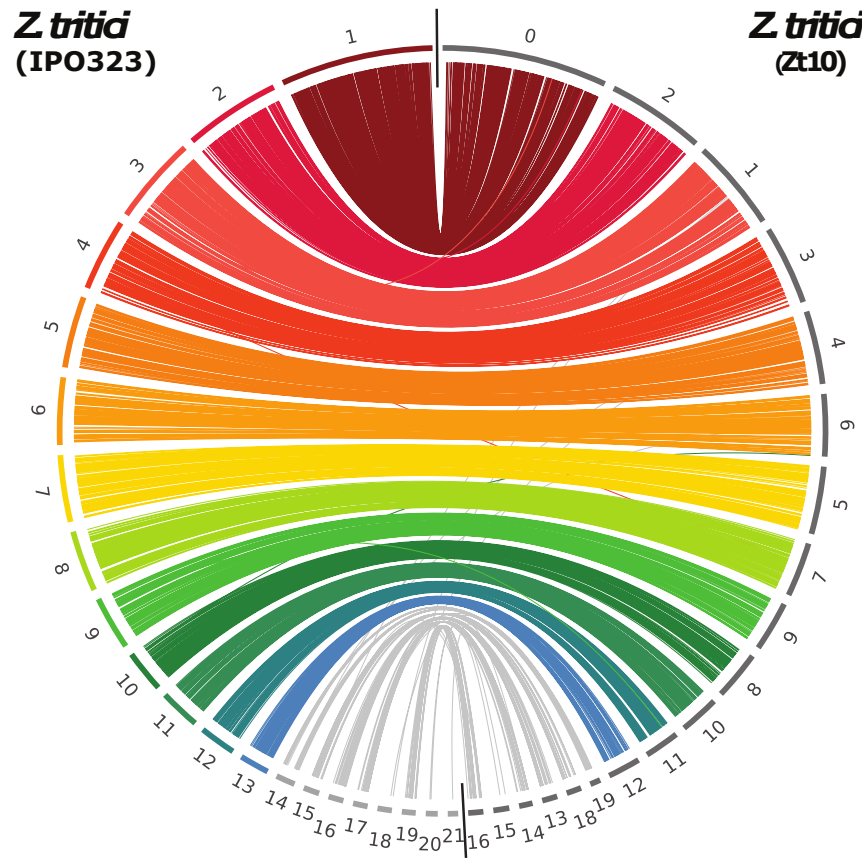
A



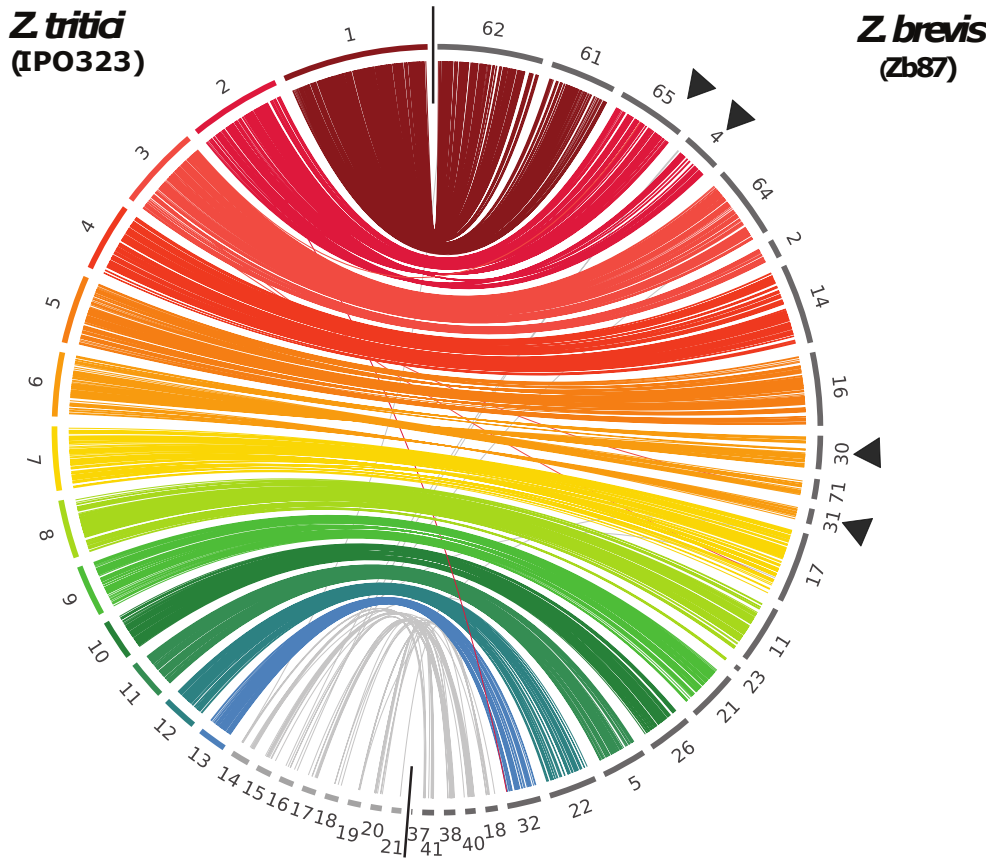
B



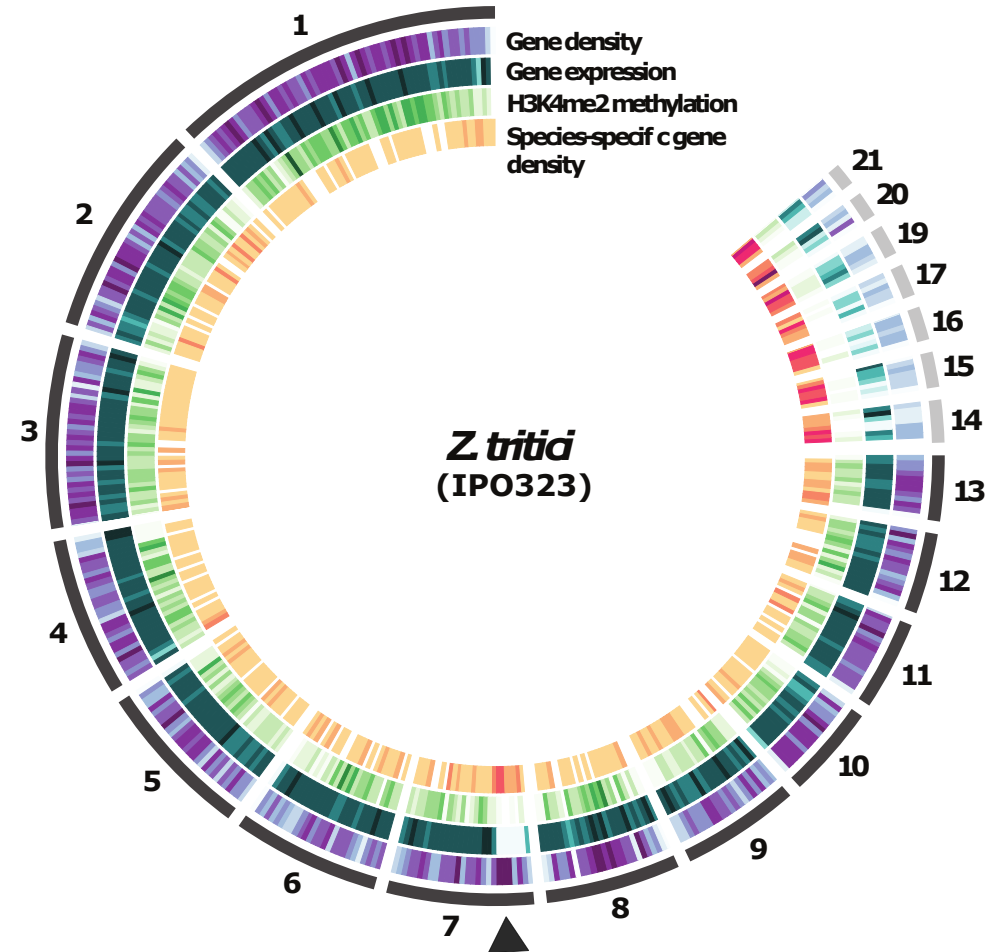
A



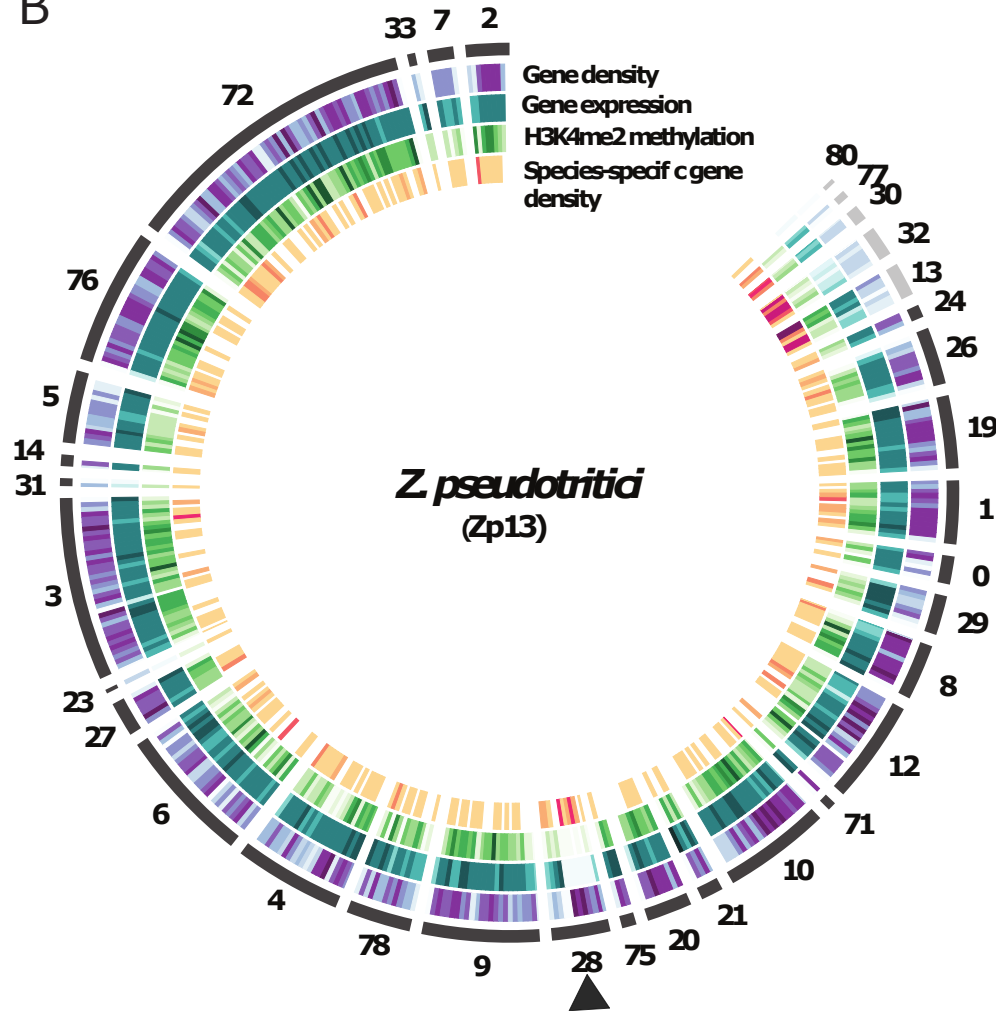
B



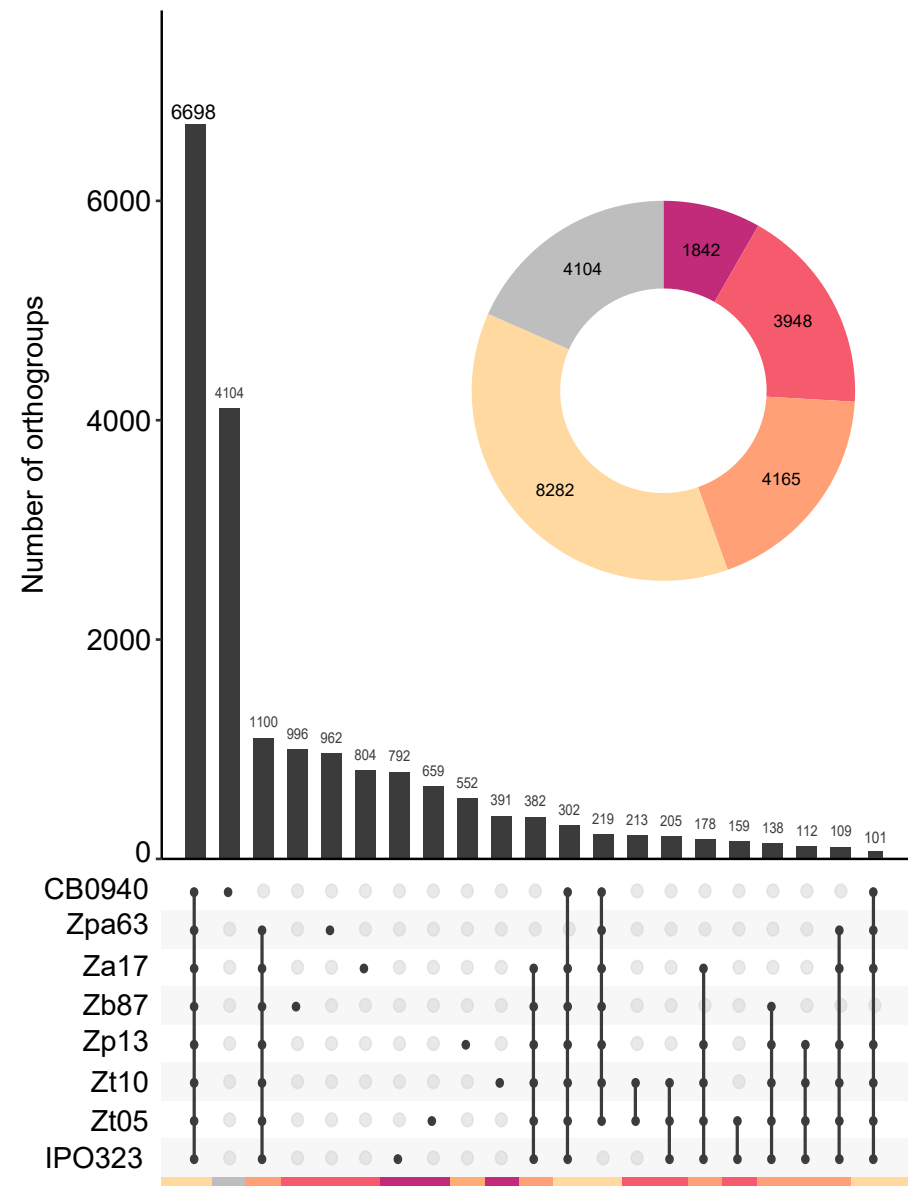
A



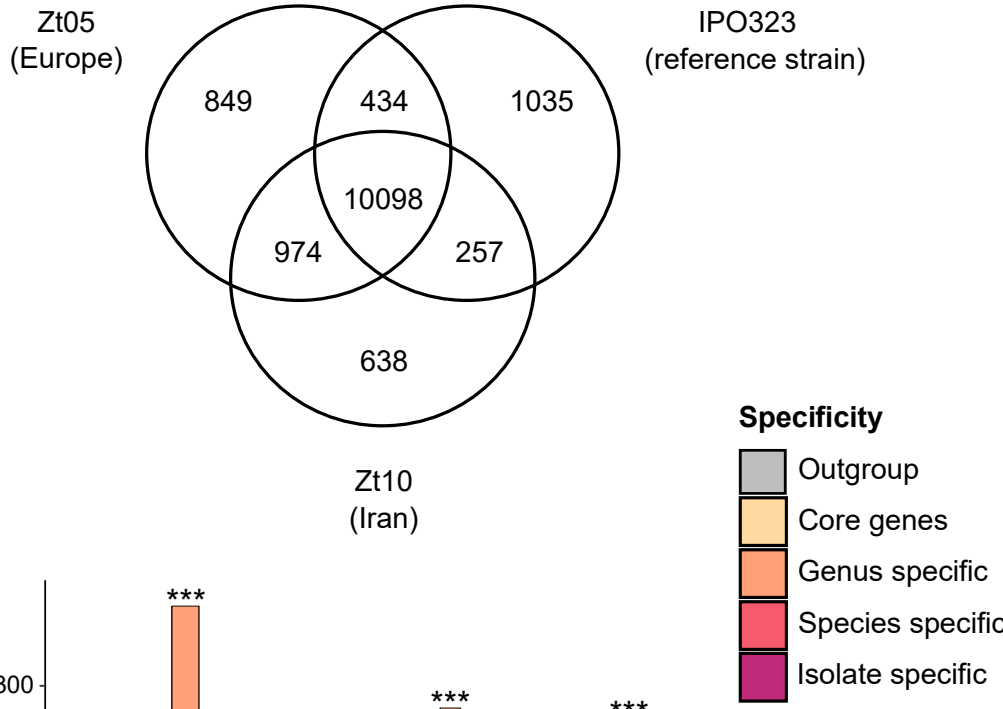
B



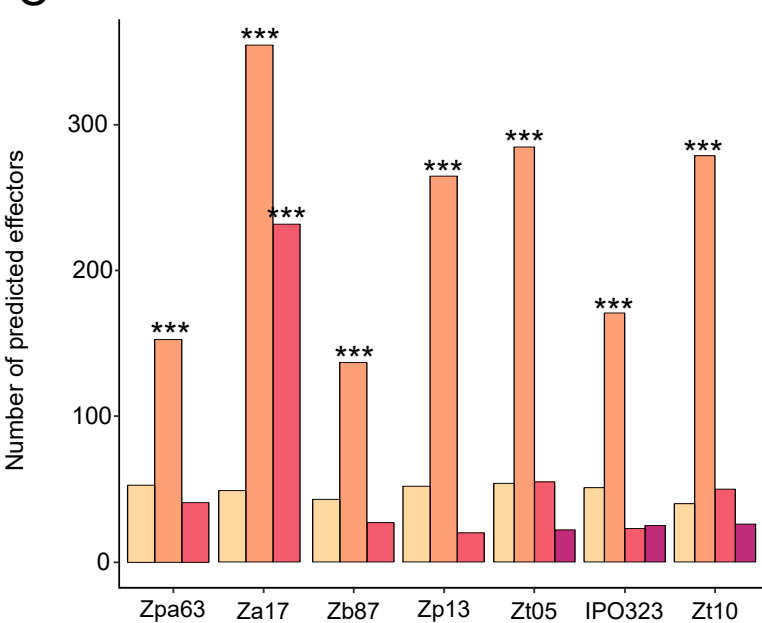
A



B

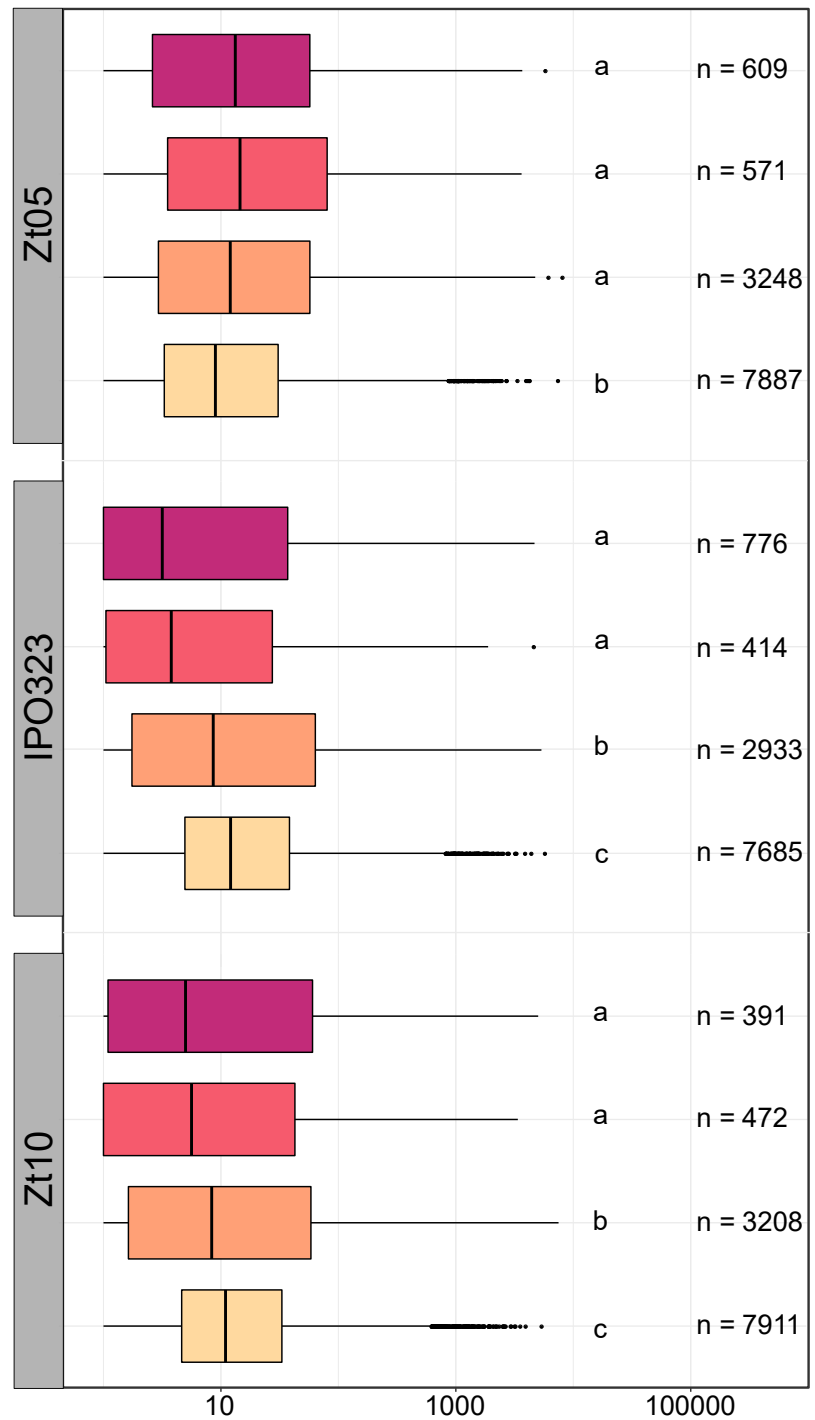


C



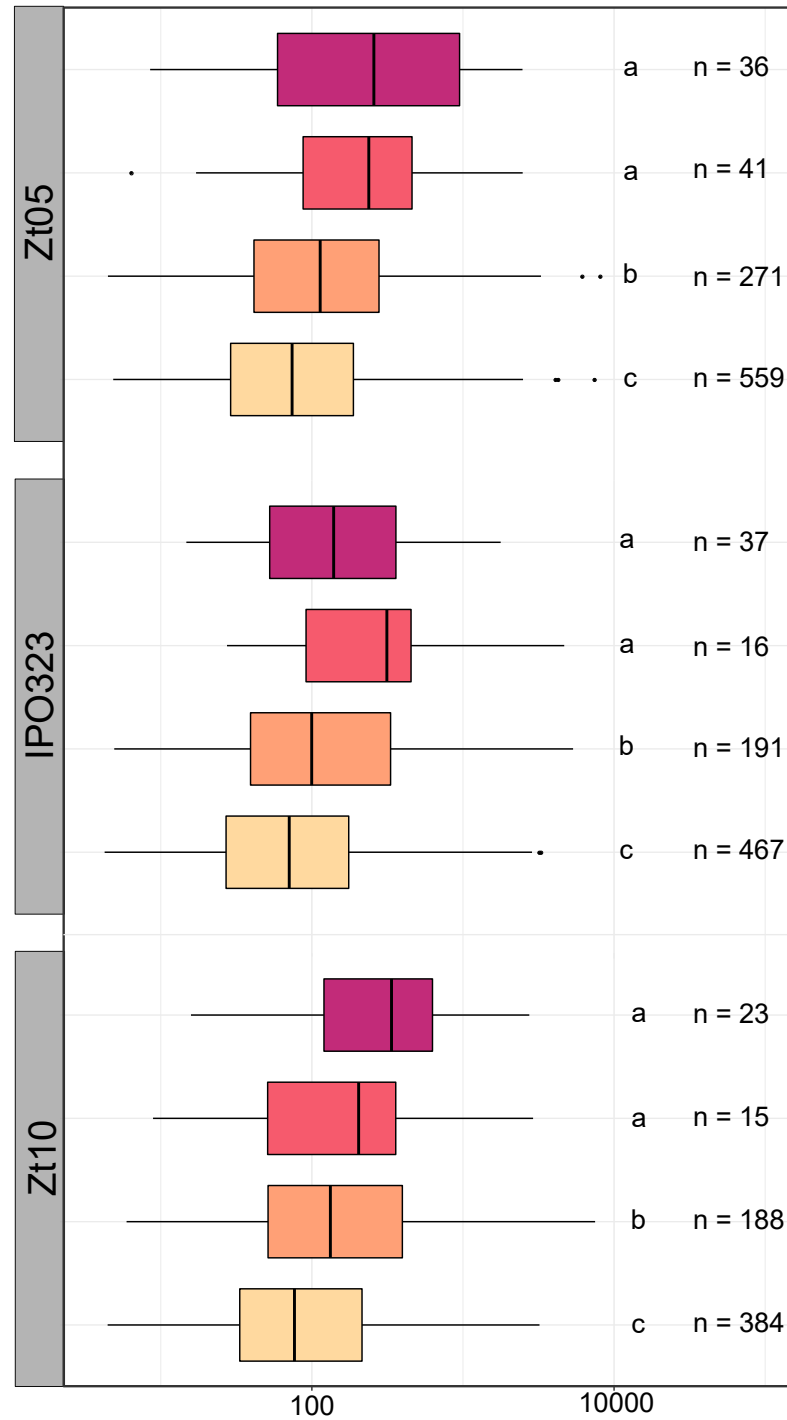
A

## Whole transcriptome



B

## Differentially expressed genes



## Specificity

- Core genes
- Genus specific
- Species specific
- Isolate specific